

Transient Hypoxia Model Revealed Cerebrovascular Impairment in Anemia Using BOLD MRI and Near-Infrared Spectroscopy

Julie Coloigner, Chau Vu, Matthew Borzage, Adam Bush, Soyoung Choi, Xin Miao, Yaqiong Chai, Cristina Galarza, Natasha Leporé, Benita Tamrazi, et al.

▶ **To cite this version:**

Julie Coloigner, Chau Vu, Matthew Borzage, Adam Bush, Soyoung Choi, et al.. Transient Hypoxia Model Revealed Cerebrovascular Impairment in Anemia Using BOLD MRI and Near-Infrared Spectroscopy. Journal of Magnetic Resonance Imaging, 2020, 52 (5), pp.1400-1412. 10.1002/jmri.27210 . inserm-02913695

HAL Id: inserm-02913695

https://inserm.hal.science/inserm-02913695

Submitted on 10 Aug 2020

HAL is a multi-disciplinary open access archive for the deposit and dissemination of scientific research documents, whether they are published or not. The documents may come from teaching and research institutions in France or abroad, or from public or private research centers.

L'archive ouverte pluridisciplinaire **HAL**, est destinée au dépôt et à la diffusion de documents scientifiques de niveau recherche, publiés ou non, émanant des établissements d'enseignement et de recherche français ou étrangers, des laboratoires publics ou privés.

Transient Hypoxia Model Revealed Cerebrovascular Impairment in Anemia using BOLD MRI and Near-Infrared Spectroscopy

Julie Coloigner PhD[1,2,†], Chau Vu MS[3,†], Matthew Borzage PhD[4,5], Adam Bush PhD[6], Soyoung Choi BA[7], Xin Miao PhD[3], Yaqiong Chai PhD[1,3], Cristina Galarza BS[8], Natasha Lepore[1,3,9], Benita Tamrazi MD[9], Thomas D. Coates MD[10,11], John C. Wood MD PhD[3,12,*]

[1]CIBORG Laboratory, Division of Radiology, Children's Hospital Los Angeles, Los Angeles, CA, USA

[2]Univ Rennes, CNRS, Inria, Inserm, IRISA UMR 6074, Empenn ERL U 1228, F-35000 Rennes, France

[3]Department of Biomedical Engineering, University of Southern California, Los Angeles, CA, USA

[4]Division of Neonatology, Fetal and Neonatal Institute, Children's Hospital Los Angeles, Los Angeles, CA, USA

[5]Department of Pediatrics, Keck School of Medicine, University of Southern California, Los Angeles, CA, USA

[6]Department of Radiology and Department of Electrical Engineering, Stanford University, Stanford, CA, USA

[7]Neuroscience Graduate Program, University of Southern California, Los Angeles, CA, USA

[8]Keck School of Medicine, University of Southern California, Los Angeles, CA, USA

[9]Department of Radiology, Children's Hospital Los Angeles, Los Angeles, CA, USA

[10]Division of Hematology-Oncology, Department of Pediatrics, Children's Hospital Los Angeles, Los Angeles, CA, USA

[11]Departments of Pediatrics and Pathology, Keck School of Medicine, University of Southern California, Los Angeles, CA, USA

[12]Division of Cardiology, Departments of Pediatrics and Radiology, Children's Hospital Los Angeles, Los Angeles, CA, USA

† Dr. Coloigner and Ms. Vu contributed equally and are designated as co-first authors.

Submission type: Original Research

Number of tables: 4

Number of figures: 6

Number of references: 40

Manuscript word count: 4813

***Correspondence:**

Dr. John C. Wood

Division of Cardiology, Mailstop 34

Children's Hospital Los Angeles

4650 Sunset Blvd

Los Angeles, CA 90027-0034

(323) 361-5470

jwood@chla.usc.edu

Acknowledgments

The authors would like to acknowledge Mr. Bertin Valdez for his efforts coordinating the patient study visits and Dr. Tom Hofstra, Dr. Jackie Bascom, Susan Carson, Trish Peterson, and Debbie Harris from the CHLA Hematology Division for their assistance with patient recruitment.

Sources of Funding

This work was supported by National Heart, Lung, and Blood Institute (grant 1U01-HL-117718-01, 1R01-HL136484-01A1 and a Minority Supplement to grant 1U01-HL-117718-01), the National Center for Research (5UL1-TR000130-05) through the Clinical Translational Science Institute at Children's Hospital Los Angeles, the National Institutes of Health (grant R01-NS074980), the National Institutes of Health Predoctoral Training in Interdisciplinary Neurosciences (1-T32-MH-111360-1-A1), National Institute of Neurological Disorders and Stroke (1F31NS106828-01A1) and National Institute of Health grant (R01-ES024936). Philips Healthcare provided support for protocol development and applications engineering on a support-in-kind basis.

Running title: Transient hypoxia model in anemia

Abstract:

BACKGROUND: Obstructive sleep apnea and nocturnal oxygen desaturations, which are prevalent in sickle cell disease (SCD) and chronic anemia disorders, have been linked to risks of stroke and silent cerebral infarcts (SCI). Cerebrovascular response to intermittent desaturations has not been well-studied and may identify patients at greatest risk.

PURPOSE: To investigate cerebral dynamic response to induced desaturation in SCD patients with and without SCI, chronic anemia and healthy subjects.

STUDY TYPE: Prospective.

SUBJECTS: 26 SCD patients (age=21±8.2, female 46.2%), including 15 subjects without SCI and 9 subjects with SCI, 15 non-sickle anemic patients (age=22±5.8, female 66.7%) and 31 controls (age=28±12.3, female 77.4%).

FIELD STRENGTH / SEQUENCE: 3T, Gradient-echo Echo-Planar Imaging.

ASSESSMENT: A transient hypoxia challenge of five breaths of 100% nitrogen gas was performed with blood-oxygen-level-dependent (BOLD) MRI and near-infrared spectroscopy (NIRS) acquisitions. Hypoxia responses were characterized by desaturation depth, time-to-peak, return-to-baseline half-life and post-hypoxia recovery in the BOLD and NIRS time courses. SCI were documented by T2-FLAIR.

STATISTICAL TESTS: Univariate and multivariate regressions were performed between hypoxic parameters and anemia predictors. Voxel-wise two-sample *t*-statistic maps were used to assess regional difference in hypoxic responses between anemic and control groups.

RESULTS: Compared to controls, SCD and chronically anemic patients demonstrated significantly higher desaturation depth ($p<0.01$) and shorter return-to-baseline timing response ($p<0.01$). Patients having SCI had shorter time-to-peak ($p<0.01$), return-to-baseline ($p<0.01$) and

larger desaturation depth (p<0.01) in both white matter regions at risk and normal appearing white matter than patients without infarcts. On multivariate analysis, desaturation depth and timing varied with age, sex, blood flow, white blood cells and cell-free hemoglobin (r^2=0.25 for desaturation depth; r^2=0.18 for time-to-peak; r^2=0.37 for return-to-baseline).

DATA CONCLUSION: Transient hypoxia revealed global and regional response differences between anemic and healthy subjects. SCI were associated with extensive heterogeneity of desaturation dynamics, consistent with extensive underlying microvascular remodeling.

Keywords: chronic anemia, sickle cell disease, silent cerebral infarct, hypoxia, gas challenge

Glossary:

SCD = sickle cell disease; **CTL** = healthy control; **ACTL** = non-sickle anemic control; **MRI** = magnetic resonance imaging; **BOLD** = blood-oxygen-level dependent; **NIRS** = near-infrared spectroscopy; **SCI** = silent cerebral infarct; **SCI+** = silent cerebral infarct positive; **SCI–** = silent cerebral infarct negative; **TTP** = time-to-peak; **T½** = half-life of return to baseline; **Δ** = change from baseline; **R** = post-challenge recovery; **DeoxyHb** = deoxygenated hemoglobin; **OxyHb** = oxygenated hemoglobin; **TotalHb** = total hemoglobin

INTRODUCTION:

Anemia is a common blood disorder characterized by decreased red blood cells, leading to low oxygen-carrying capacity and reduced delivery of oxygen to the tissue (1). Anemia is the hallmark of several common genetic diseases, including sickle cell disease (SCD) and thalassemia.

Since the brain is exquisitely sensitive to interruptions in oxygen supply, previous studies have shown that both acquired and congenital anemias, including thalassemia and sickle cell anemia, are often associated with higher risk of stroke and silent cerebral infarcts (SCI) (2,3). Among many stressors connected to the etiology of SCI, obstructive sleep apnea and nocturnal desaturation have been linked to cerebrovascular accidents in SCD and anemic patients (4,5). Even though apnea-related low oxygenation levels and frequent hypoxia episodes are likely contributing factors to the increased stroke risks in chronically anemic subjects, the dynamics of these desaturations has not been well studied.

This present work explored the brain's dynamic response to hypoxia using two methods: near-infrared spectroscopy (NIRS) and blood-oxygen-level-dependent (BOLD) MRI. NIRS is an optical imaging technique that measures tissue oxygen saturation based on the difference in transmitted and received photons at near-infrared wavelengths (6). On the other hand, functional BOLD MRI measures subtle changes in regional cerebral deoxyhemoglobin concentration consequent to the modulation of neural metabolism; BOLD MRI is frequently used as a biomarker for disease or evaluation of clinical therapies (7).

Thus, the goal of this study was to compare cerebrovascular responses to a transient hypoxia exposure in a patient population (sickle cell disease) enriched for both SCI and obstructive sleep apnea, using patients with non-sickle anemia to control for the effects of decreased hemoglobin alone as well as normal control subjects for reference.

MATERIALS AND METHODS:

Study population:

The Committee on Clinical Investigation at Children's Hospital Los Angeles approved the protocol; written informed consent and/or assent were obtained from all subjects. This study was performed in accordance with the Declaration of Helsinki.

A total of 72 subjects were enrolled between January 2012 and May 2017. Exclusion criteria were the following: 1) pregnancy; 2) hypertension; 3) diabetes; 4) overt stroke or other known neurologic insult; 5) seizures; and 6) known developmental delay or learning disability. Patients with previously identified SCI were allowed to participate. As defined by the Silent Cerebral Infarct Multi-Center Clinical Trial (SIT), an SCI is an MRI signal abnormality that was equal or greater than 3mm in diameter and visible on two orthogonal planes on T2-FLAIR images and no associated neurological symptoms (8).

Only subjects older than 12 years of age were included in the study. Imaging, vital signs and blood samples were obtained on the same day for each subject. Complete blood count and quantitative hemoglobin electrophoresis were analyzed in our clinical laboratory. All chronically transfused patients were studied on the same day of their blood transfusion, prior to receiving blood, when their hemoglobin levels were at the nadir.

The first patient group consisted of 26 SCD subjects: 19 subjects with homozygous hemoglobin S (HbSS), 7 subjects with heterozygous combination of hemoglobin S and hemoglobin C (HbSC) and 5 subjects with heterozygous hemoglobin S and a β_0 thalassemia mutation (HbSβ_0) which behaves similarly to the HbSS mutations. The second group consisted of 15 patients with non-sickle chronic anemia disorders who did not suffer from any other known medical conditions apart from their chronic anemia (referred to as anemic controls, ACTL). The

third group consisted of 31 African and Hispanic American healthy controls (CTL). Most controls were first or second-degree relatives of the SCD patients in order to ensure a similar economic and social background compared to the patient group. Therefore, sickle cell trait was common among control subjects; these were subjects who had approximately 40% of hemoglobin S (HbS) in their blood but no cells containing exclusively HbS.

Hypoxia gas challenge:

The experimental setup is illustrated in Figure 1. At the start of the image acquisitions, patients were breathing through a two-liter reservoir rebreathing circuit supplied by pressurized, non-humidified room air at 12 liters per minute. This system included one-way valves to prevent partial gas mixtures and respiratory bellows (Invivo Corporation, Gainesville, FL) to display the breathing pattern and frequency. At 50 seconds into the data acquisition, the room air gas mixture was switched to 100% nitrogen until the patient had completed 5 breaths (approximately 25 seconds), then the circuit was changed back to room air. Peripheral arterial oxygen saturation (S_pO_2) were acquired by fingertip pulse oximetry concurrently with forehead NIRS and BOLD MRI during the gas challenge.

Near-infrared spectroscopy (NIRS):

A NIRS system (NIRO-200 system, Hamamatsu Photonics, Hamamatsu City, Japan) was used to measure relative changes of oxygenated hemoglobin (OxyHb) and deoxygenated hemoglobin (DeoxyHb) in the frontal cerebral circulation continuously throughout the hypoxia challenge (6). The NIRS system operated with three wavelengths of light (775, 810 and 850nm). The probes were placed on the side of the subject's forehead just above the eyebrow. These NIRS

signals were acquired at 1kHz and synchronized to the BOLD acquisitions via a Biopac MP150 data acquisition system (BioPac, Goleta, CA). A modified Beer-Lambert law was used to calculate the relative change in oxygenated hemoglobin (OxyHb), deoxygenation hemoglobin (DeoxyHb) and total hemoglobin (TotalHb, equivalent to the sum of OxyHb and DeoxyHb).

Magnetic resonance imaging:

Each participant underwent an MRI study using a 3T Philips Achieva with an 8-element phased-array coil. A 3D T1-weighted image was acquired covering the whole brain (160 sagittal slices) with TR = 8ms, TE = 4ms, flip angle = 8°, in-plane resolution = 1mm × 1mm, FOV = 256mm × 256mm and slice thickness = 1.0mm. T2-weighted fluid-attenuated inversion recovery (T2-FLAIR) 3D image was acquired with the following parameters: TR = 4800ms, TE = 257.9ms, TI = 1650ms, in-plane resolution = 1mm × 1mm, FOV = 256mm × 256mm and slice thickness = 1.3mm. BOLD images were acquired using gradient-echo echo-planar-imaging sequence: TR = 2000ms, TE = 50ms, in-plane resolution = 2.3mm × 2.3mm, FOV = 220mm × 220mm, 26 axial slices, slice thickness = 5mm, SENSE factor of 2. A total of 150 volumes were collected in five minutes. To measure global cerebral blood flow, a phase contrast MRI was also obtained, positioned just above the carotid bifurcation: TR = 1286ms, TE = 77ms, FOV = 220mm × 220mm, resolution = 1.2mm × 1.2mm, velocity encoding gradient of 200mm/s and slice thickness = 5mm. MR angiography image was acquired: TR = 23ms, TE = 3.45ms, flip angle = 18°, FOV = 220mm × 220mm, resolution = 0.38mm × 0.38mm and slice thickness = 1.4mm.

Definitions of dynamic parameters of NIRS and BOLD hypoxia response:

Different parameters for hypoxia dynamics were defined from the NIRS and BOLD responses in hypoxia, which were modeled by a piecewise function: an affine function during desaturation and an exponential function during recovery.

The following definitions of hypoxic parameters were provided for DeoxyHb but without loss of generality were used to compute response dynamics for OxyHb and BOLD time series:

(1) $\mathbf{DeoxyHb_{hypoxia}}$ measure was defined as the peak absolute value of DeoxyHb measured in the entire challenge duration.

(2) $\mathbf{DeoxyHb_{pre\text{-}hypoxia}}$ was the mean DeoxyHb signal before hypoxic gas, calculated from the start of the sequence to the start of nitrogen gas administration at 50 second.

(3) $\mathbf{DeoxyHb_{post\text{-}hypoxia}}$ was the mean signal after the signal has returned to baseline; because typical hypoxia effects do not last past 100 seconds following the start of gas administration, the post-hypoxia period was defined from 120 seconds to the end of the sequence.

(4) $\Delta_{\mathbf{DeoxyHb}}$ (the depth of the hypoxic change, μmol) was calculated as $\Delta_{DeoxyHb} = |DeoxyHb_{pre\text{-}hypoxia} - DeoxyHb_{hypoxia}|$.

(5) $\mathbf{TTP_{DeoxyHb}}$ (time-to-peak) was defined as the duration between the start of desaturation response to the peak $DeoxyHb_{hypoxia}$ signal.

(6) $\mathbf{T½_{DeoxyHb}}$ (half-life of the return to baseline) was the time for the hypoxia signal to recover 50% of the previous signal change. The transition time points (time at onset of hypoxia and end of hypoxia) were determined by iterating through and selecting the time points with the lowest least-squares error compared to the piecewise model.

(7) $\mathbf{R_{DeoxyHb}}$ was the signal recovery level computed as $R_{DeoxyHb} = DeoxyHb_{post\text{-}hypoxia} - DeoxyHb_{pre\text{-}hypoxia}$. This signal was not computed for the BOLD time series due to confounds from low-frequency drifting during the five-minute acquisition.

Regarding the BOLD signal, the same measures were calculated for each voxel of the BOLD time series, normalized by baseline $BOLD_{pre\text{-}hypoxia}$. Pictorial illustrations of these definitions can be found in Figure 2D.

Image processing:

Structural T1 images were registered to the Montreal Neurological Institute (MNI) template with the FMRIB Software Library (FSL); BOLD images were preprocessed with FSL and registered to MNI template space using a standard spatial functional pipeline (9).

Global hypoxic parameters were computed as an average within a whole-brain mask in the MNI template. MNI-based grey matter mask, an eroded white matter mask and three vascular territories masks were used to calculate average BOLD hypoxic responses for these different brain regions. The white and grey matter masks were generated out of the Colin 27 Average Brain white matter and grey matter templates (10). The white matter mask was eroded using a 2mm Gaussian kernel to avoid the partial volume effect. Masks of the anterior cerebral artery, middle cerebral artery and posterior cerebral artery circulations were based on the published templates of vascular territories in both hemispheres (11).

Baseline cerebral blood flow:

Whole-brain cerebral blood flow was measured using phase contrast MRI (12). A single, two-dimensional phase contrast slice was positioned approximately 1 to 5cm superior to the carotid bifurcation with the aim of optimal orthogonality to the carotid and vertebral arteries. Vessel boundaries were semi-automatically segmented from the complex difference images using Canny edge detection and mapped to the phase difference image for blood flow calculation.

Clinical MR Imaging:

MR angiography for identification of vasculopathy and T2-FLAIR images for identification of SCI were reviewed by three observers blinded to disease status: BT (12 years of experience), JCW (10 years of experience) and SC (10 years of experience). Discrepancies were resolved by simultaneous viewing with consensus.

Silent cerebral infarcts (SCI) analysis:

Semi-manual segmentation of individual SCI was performed on T2-FLAIR in a previous study on the same patient cohort (13). Each SCI lesion volume and centroid on the MNI template were saved for statistical analysis. The segmentations were then fused to create a SCI density map that localized SCIs across all the SCD subjects. In order to explore the effect of silent strokes, the SCD group was split into two subgroups: subjects without infarcts (SCI–) and subjects with abnormal infarcts (SCI+). The ACTL group was not subdivided because the group size was too small.

To determine spatial co-localization between BOLD parameters and silent infarct distribution, we performed permutation analysis of SCI on desaturation depth and timing two-sample *t*-maps (13). To minimize the bias caused by the BOLD signal within the dead tissue of an infarction, this permutation analysis was not performed on individual subject's maps, but the group maps in which areas with SCI presence constituted lesion-prone regions – or regions more vulnerable to SCI development. The reference signal was computed as the mean values within the original infarct positions on the map. To generate a robust background signal for the null statistic, 100 permutation operations were performed, each placing an infarct centroid in a random location

within an eroded white matter mask and calculating the mean values in the displaced volume. Two-tailed two-sample *t*-tests were performed between BOLD parameters derived from normal appearing regions and regions vulnerable to silent infarcts.

Statistical analysis:

Statistical analysis on global desaturation values was performed in JMP (SAS, Cary, NC). One-way ANOVA with Dunnett's post hoc correction was used to examine the difference in clinical and hypoxic variables between SCD and control, and between ACTL and control; independent samples *t*-test was used to compare SCD and ACTL patient groups. Univariate and stepwise multivariate regressions were performed against predictors of anemia and SCD severity, including age, sex, hemoglobin, cerebral blood flow, presence of SCI, transfusion status, white blood cell count, platelet count, reticulocytes, fraction of S-cells, fetal hemoglobin and cell-free hemoglobin level. These predictors have been demonstrated to be characteristic of the pathophysiology of SCD and chronic anemia disorders (3,14–18). All variables having univariate $p<0.10$ were included as candidates for stepwise multivariate analysis. Variables were retained in the final model for $p<0.05$.

Pearson correlation tests were performed on Δ_{BOLD}, T½, TTP and R against hemoglobin level and S_pO_2. The resulting *p*-values were corrected for multiple comparisons using False Discovery Rate Benjamini-Hochberg method, with $q=0.05$.

Voxel-wise effect size tests were performed to generate a Cohen's *d*-map in each patient group. Cohen's *d* was calculated by $d = \overline{\Delta_{BOLD}} / s_{baseline}$, with $\overline{\Delta_{BOLD}}$ as the group mean desaturation depth and $s_{baseline}$ as the standard deviation of the normalized baseline. Two-sample *t*-maps were generated with Analysis Functional NeuroImages (AFNI) to compare desaturation

parameters between controls and SCD or ACTL patients; *t*-statistic was calculated by $t = (\overline{x_{SCD/ACTL}} - \overline{x_{CTL}}) / (s_p \sqrt{\frac{1}{n_{SCD/ACTL}} + \frac{1}{n_{CTL}}})$, with $n_{SCD/ACTL}$ and n_{CTL} as group sizes, $\overline{x_{SCD/ACTL}}$ and $\overline{x_{CTL}}$ as parameter means, $s_{SCD/ACTL}$ and s_{CTL} as parameter standard deviations and s_p as the pooled standard deviation $s_p = \sqrt{\frac{(n_{SCD/ACTL}-1)\, s^2_{SCD/ACTL} + (n_{CTL}-1)\, s^2_{CTL}}{n_{SCD/ACTL} + n_{CTL} - 2}}$.

RESULTS:

Demographics:

Table 1 summarizes the demographics of the three participating groups. The SCD and ACTL groups were matched for age and sex but the healthy controls were older (p<0.01) and had a higher proportion of females (p=0.03). Therefore, age and sex were included as independent variables in all regression analyses. No significant difference was observed in the NIRS and global BOLD dynamics between control subjects with sickle cell trait and non-trait control subjects (p=0.43 for Δ_{BOLD}, p=0.77 for Δ_{OxyHb} and p=0.40 for $\Delta_{DeoxyHb}$). None of the patients consciously perceived the desaturation episode and no complications were encountered. The BOLD imaging and fingertip S_pO_2 were acquired on all three subject groups. Due to sensor malfunction, the NIRS analysis only retained 19 SCD patients, 24 controls and 12 ACTL patients out of 72 subjects in the study cohort.

Hematologic markers:

Compared to anemic patients, control subjects had higher hemoglobin concentration (p<0.01), higher hematocrit (p<0.01), lower cell-free hemoglobin level (p<0.01) and lower cerebral blood flow (p<0.01). The SCD and ACTL groups were well matched for hemoglobin

(p=0.78) and cell-free hemoglobin levels (p=0.62), but the SCD patients had higher reticulocytes (p=0.03), white blood cells count (p<0.01), fetal hemoglobin (p=0.02) and fraction of S-cells (p<0.01). Out of 26 SCD patients, 46.2% were transfused compared to 80.0% in the ACTL patients. Within the SCD group, the median HbS percentage was 67.2% in the non-transfused group and reduced to 15.3% in the transfused group.

Clinical MR imaging:

Based on MR angiography, only 1 SCD patient had severe bilateral anterior cerebral artery stenosis. Although no subject had a history of stroke, T2- FLAIR imaging demonstrated SCIs in 3 in control patients (9.7%), 9 in SCD patients (34.6%, p=0.05) and 2 in ACTL patients (13.3%, p=1.00), as described in Table 1.

Pulse oximetry and NIRS dynamics:

Figure 2A shows a typical S_pO_2 measurements during the challenge, demonstrating similar depth and duration to spontaneous desaturations during anatomic scanning when the subject was sleeping (Figure 2B). The nitrogen challenge produced minimum S_pO_2 values of 78.8 ± 9.8%. The ΔS_pO_2 measure was strongly correlated with hemoglobin levels (r^2=0.37, p<0.01).

Group average NIRS parameters are summarized in Table 2. Both Δ_{OxyHb} and $\Delta_{DeoxyHb}$ were correlated with ΔS_pO_2 (r^2=0.21, p<0.01 for Δ_{OxyHb}; r^2=0.30, p<0.01 for $\Delta_{DeoxyHb}$). The depth $\Delta_{DeoxyHb}$ was associated with hemoglobin level (r^2=0.11, p=0.04), but Δ_{OxyHb} was not. The T½ for both oxyhemoglobin and deoxyhemoglobin were shorter in anemic subjects (p=0.04 and p<0.01 respectively) and correlated with hemoglobin (r^2=0.11, p=0.02 for OxyHb; r^2=0.18, p<0.01 for DeoxyHb), but TTP was not different in anemic subjects. Compared to pre-hypoxia baseline, all

three groups demonstrated a decrease in R_{OxyHb} (p<0.01) and a rise in both $R_{DeoxyHb}$ (p<0.01) and $R_{TotalHb}$ (p<0.01). The $R_{TotalHb}$ level was correlated with resting hemoglobin concentration (Figure 3A), with patients with significantly lower hemoglobin exhibiting a deficit in the capability to increase total hemoglobin in response to hypoxia.

Global BOLD dynamics:

Similar to the NIRS analysis, a larger drop in S_pO_2 correlated with higher BOLD changes (r^2=0.50, p<0.01) and shorter timing dynamics (r^2=0.42, p<0.01). The Δ_{BOLD} was negatively correlated with resting hemoglobin level (r^2=0.09, p=0.04) as illustrated in Figure 3B. Group average BOLD parameters are shown in Table 2, and hypoxic parameters within different tissue types and arterial territories are shown in Supplemental Table S1.The SCD and ACTL groups displayed a deeper desaturation in the white matter (p<0.01) and grey matter (p<0.01) compared to healthy controls. T½ for white matter (p<0.01), grey matter (p<0.01) and arterial perfusion territories (p<0.01 for all three territories) were shorter for SCD group in comparison with controls. Strong associations were also observed between the Δ_{BOLD}, $T½_{BOLD}$, TTP_{BOLD} and corresponding DeoxyHb and OxyHb signals (Figures 3C and 3D). $T½_{BOLD}$ demonstrated a strong association with hemoglobin (r^2=0.19, p<0.01) but TTP_{BOLD} had no relationship with hemoglobin level.

Classic risk factors for SCD and anemia as predictors of global BOLD dynamics:

Table 3 summarizes the univariate and multivariate predictors for the global values of $T½_{BOLD}$, TTP_{BOLD} and Δ_{BOLD}. Patient sex (p=0.03) and cell-free hemoglobin levels (p=0.03) were the only significant predictors of TTP, and both were retained on multivariate analysis (combined r^2=0.18). Out of 12 regressors listed, 9 predictors were correlated with $T½_{BOLD}$ on univariate

analysis, but only cerebral blood flow and white blood cell count remained significant on multivariate analysis (combined r^2=0.37). Univariate predictors of Δ_{BOLD} were age, cerebral blood flow, hemoglobin, transfusion status, tissue oxygenation and white blood cell count, but only age and white blood cell count were retained after multivariate analysis (combined r^2=0.25).

Effects of hemoglobin on regional variations in BOLD signal:

Figure 4A displays the group average Δ_{BOLD} maps in representative axial and sagittal views in the three patient groups. Similar to global Δ_{BOLD}, regional Δ_{BOLD} dynamics also had significantly larger depth in SCD and ACTL compared to control subjects, with greater between-group differences observed in the grey matter compared to the white matter. With similar baseline BOLD variability between subject groups, SCD and ACTL patients showed larger Cohen's *d*-values compared to healthy controls (Figure 4B).

In examining the voxel-wise hypoxic dynamics between anemic and healthy subjects, two-sample *t*-maps of Δ_{BOLD}, $T½_{BOLD}$ and TTP_{BOLD} between SCD patients and healthy controls were shown in Figure 5A, and between ACTL patients and healthy controls in Figure 6. Generally, *t*-scores for $T½_{BOLD}$ and TTP_{BOLD} were less than zero, indicating shorter regional timing response parameters in SCD patients compared to controls. After adjusting for hemoglobin, age and sex, both $T½_{BOLD}$ and TTP_{BOLD} maps had many more normal *t*-scores but spatial variability remained higher than expected (Figure 5B).

Insight into this observation was provided by plotting hemoglobin-corrected two-sample *t*-maps separately for SCI– (Figure 5C) and SCI+ patients (Figure 5D) compared with healthy controls. The Δ_{BOLD}, $T½_{BOLD}$, and TTP_{BOLD} *t*-maps for SCI– subjects were spatially homogenous and had relatively few abnormal *t*-scores (0.54%, 1.30% and 0.12% of voxels with $|t|>2$

respectively). In contrast, *t*-score maps from patients who were SCI+ demonstrated marked spatial heterogeneity and more severe *t*-score extremes in both positive and negative directions (13.1%, 10.6% and 4.5% of voxels with $|t|>2$ respectively). SCI+ patients had markedly prolonged $T½_{BOLD}$ in the right anterior and middle cerebral arteries distribution and shorter in the left anterior cerebral artery and middle cerebral artery distribution (Figure 5D and Supplemental Figure S2). The TTP_{BOLD} measures remained shortened in the frontal regions and were abnormally increased in the posterior region distribution in SCD patients (Supplemental Figure S2). Voxel-wise two-sample *t*-maps are shown for ACTL group in Figure 6, with a distribution of abnormal *t*-scores in their Δ_{BOLD}, $T½_{BOLD}$, and TTP_{BOLD} *t*-maps (10.4%, 2.5% and 2.4% of voxels with $|t|>2$ respectively). However, the hypoxic timing responses in ACTL were less spatially heterogenous compared to the SCD group (Figure 6 and Supplemental Figure S2).

Table 4 summarizes the permutation results computed on the hemoglobin-corrected *t*-maps for SCI– and SCI+ sickle-cell patients. SCI+ patients had slightly shorter $T½_{BOLD}$, markedly shorter TTP_{BOLD} and deeper Δ_{BOLD} in both white matter regions at risk and normal appearing white matter than SCI– patients. In SCI+ patients, regions at risk for stroke had shorter TTP_{BOLD} and smaller Δ_{BOLD} than normal appearing white matter, while the converse was true in SCI– patients. $T½_{BOLD}$ was longer in regions at risk for stroke for patients in both subgroups.

DISCUSSION:

Using concurrent measurement of NIRS and BOLD MRI during a desaturation gas challenge, the present work investigated the human dynamic brain response to transient hypoxia. This state of induced hypoxia mimics nocturnal desaturation – a common disorder in SCD and chronic anemia disorders linked to increased risks for strokes and cardiovascular diseases (4,5).

Our results revealed that anemic patients experienced deeper global oxygen desaturation and shorter half-time of recovery consistent with their higher blood flow. We demonstrated striking differences in the timing and depth of the desaturation between anemic patients and controls, especially between SCI+ and SCI– sickle-cell patients. The patients with SCI exhibited pronounced spatial heterogeneity in these comparative maps, notably anterior-posterior variations in TTP maps and left-right variations in T½ maps. In these patients, regions at high risks for infarcts were associated with slower saturation recovery despite a shorter time to peak desaturation suggestive of local micro-vascular obstruction.

Our short and well-tolerated hypoxia protocol (19) behaved similarly to dynamic susceptibility contrast MRI except the signal loss was caused by increased concentration of paramagnetic deoxygenated hemoglobin rather than an exogenous contrast agent. Transient hyperoxia has been used as a magnetic tracer (20), but use of transient hypoxia has not been described in humans. Comparison of this transient hypoxia model between NIRS and BOLD time courses showed strong inter-modality correlation (21); this was reassuring since NIRS predated BOLD and was a well-validated tool in tissue oxygenation measurement (6). The strongest correlation was observed between Δ_{BOLD} and $\Delta_{DeoxyHb,}$ rather than $R_{TotalHb}$ (21), suggestive of hemoglobin deoxygenation as the initial hypoxic response before blood flow changes; this observation was in line with previous work which showed more rapid deoxyhemoglobin-sensitive R_2* changes during hypoxia compared to cerebral blood flow (22). The depth and time course of NIRS and BOLD response paralleled the S_pO_2 signal, suggesting that cerebral metabolic rate and blood flow were relatively stable over the period of transient hypoxia despite the small rise in $R_{TotalHb}$. To place the predicted flow changes into perspective, step changes of inhaled oxygen from room air to pO_2 of 50 torr lowered oxygen saturation to 80% (comparable to the desaturations in

this study) and increased brain blood flow by 10% (23). However, the time constant of response was 79.6±29.2 seconds, so approximately 25 seconds of exposure is likely to trigger a much smaller response.

Using these empiric parameters, we demonstrated abnormal blood flow, resistance and compliance of the vascular bed in the anemic patients. We contend that the higher Δ_{BOLD}, shorter TTP_{BOLD} and shorter $T½_{BOLD}$ in anemic patients reflect lower cerebrovascular resistance and serve as a compensatory mechanism for higher blood flow. These changes were greatest in the grey matter, probably as a result of increased capillary density in the cerebral cortex in chronically hypoxic patients (24). Neovascularization is more hindered in the white matter, potentially explaining the more muted changes there (24).

While TTP_{BOLD} and $T½_{BOLD}$ reflect many factors, increased $R_{TotalHb}$ is specific for compensatory vasodilation which is triggered when partial pressure pO_2 falls below 50mmHg (25). The $R_{TotalHb}$ was positive in most healthy subjects but blunted in anemic subjects, potentially reflecting exhaustion of vasodilatory reserve (26). Hypoxic challenge, however, has been demonstrated to cause greater increases in minute ventilation in anemic subjects (27), and the corresponding decrease in end-tidal CO_2 could partially counter hypoxic vasodilation. Subsequent studies with controlled end-tidal CO_2 concentration are warranted to eliminate contributions from exaggerated respiratory compensation to $R_{TotalHb}$ changes.

In multivariate regression analyses of global desaturation parameters, the dependence of Δ_{BOLD} on age is physiologically understandable, as vascular resistance tends to increase monotonically with age in many disease states including SCD (3,16,28). Similarly, the association between shorter timing dynamics and higher cerebral blood flow was also more likely a physiologic than pathologic statistical association. The association between microvascular flow

dynamics and white blood cell count had been previously demonstrated in the Cooperative Study of Sickle Cell Disease (15). The association between increased cell-free hemoglobin and male sex with global BOLD timing was consistent with disease severity as cell-free hemoglobin had been shown to correlate with systemic endothelial dysfunction in SCD (29) and male sex with higher blood pressure and higher stroke rate (30).

The striking spatial heterogeneity in the timing and depth of the desaturation, particularly the SCI+ subgroup is likely a marker of heightened capillary transit time heterogeneity (31), which is frequently observed in progressive microvascular diseases (32). The increased baseline blood flow in chronic anemias tends to worsen the transit time heterogeneity, leading to impaired regional oxygen extraction and exposing these patients to ischemic injury during periods of restricted oxygen delivery (31). This microvascular impairment and heterogeneity was consistent with previous works that demonstrated diffuse abnormalities in regional cerebral blood flow in sickle-cell patients lacking overt stroke or abnormal angiography (13,33). T½ maps were particularly prolonged in infarct prone white matter regions in deep watershed areas, consistent with reports of increased oxygen extraction fraction in these regions in SCD patients (34). Previous work using hypercapnia challenges in the elderly has also suggested that blunted cerebrovascular responsiveness is ominous even in non-anemic subjects (35), progressing to SCI even in otherwise normal appearing white matter (36).

If regional CBF were completely constant throughout the hypoxic stimulus changes, one would expect variations in $T½_{BOLD}$ and TTP_{BOLD} to be highly correlated. However, hypoxia could potentially produce blood flow redistribution to favor important structures. PET data suggests that phylogenetically older brain regions, preferentially supplied by the posterior circulation, are better protected and show higher increase in CBF in response to hypoxia than middle and anterior brain

regions (37). Anemia could be exaggerating this physiologic redistribution, explaining the shorter $T½_{BOLD}$ and prolonged TTP_{BOLD} in the posterior circulation of anemic subjects compared to controls. Selective reduction of vascular resistance in the posterior circulation could create a physiological steal phenomenon (38) which would leave the anterior and middle cerebral artery territories with lower flow and longer $T½_{BOLD}$ post-hypoxia. Physiological steal could also explain the higher stroke rate observed the anterior circulation compared to posterior territory (39).

A large fraction of the NIRS and BOLD response to hypoxia could be explained by differences in pulse oximetry response to the nitrogen challenge. Since chronically anemic patients tended to have higher cardiac output and pulmonary blood flow to compensate for their decreased oxygen carrying capacity, oxygen washout during nitrogen inhalation in the lungs was increased, causing greater hemoglobin desaturation. The larger hemoglobin desaturation led to a larger effect size observed in S_pO_2 and BOLD hypoxic signal changes. This observation was corroborated by the positive association between baseline blood flow and Δ_{BOLD} in our work and the correlation between the oximetry desaturation depth and hemoglobin in previous animal work (27).

Limitations:

A limitation to our study was the uncorrectable variations in the patient tidal volume and minute ventilation that influenced individual desaturation depth. Intra-subject variability in exposure made it difficult to interpret individual parameter maps. End-tidal CO_2 sensors were built into the breathing circuit, but technical difficulties prevented us from using these data. Previous work has shown that hematocrit affects the BOLD signal (40), thus potentially influencing the parameter estimation in SCD and anemic subjects. The desaturation signal could have also been confounded by the lower signal-to-noise ratio within the vicinity of the SCI, which confounded

the difference in hypoxic parameters observed between SCI-prone regions and normal appearing white matter. Additionally, even though multivariate regression analyses of global desaturation parameters yielded several classic risk factors for anemia and sickle cell disease severity, our study was underpowered to detect these correlations within individual subject groups.

Furthermore, we could not standardize the hypoxic dosage with our current equipment since the nadir of the pulse oximetry measurement is reached 15-20 seconds after the patient is switched back to room air, so we could not use the pulse oximeter to titrate the hypoxia to consistent depths. It is likely that the use of a controlled respirator such as the RespirAct system (Toronto, ON, Canada) could achieve more consistent hypoxia exposures. In addition, the bolus timing parameters (T½, TTP) were primitive and indirect metrics of cerebral blood flow; the addition of post-processing tools designed for dynamic susceptibility contrast to our controlled hypoxia design could yield contrast-free voxel-wise mappings of relative cerebral blood volume, blood flow and mean transit time in the brain.

Conclusion:

Our data suggested that SCI represented an iceberg phenomenon with respect to microvascular damage, namely that the presence of infarcts reflected much more extensive underlying microvascular remodeling. This observation was concordant with the 14-fold increase in relative stroke risk associated with SCI and raised the question of whether routine screening for SCI should be performed for sickle-cell patients (14). Looking forward, the striking regional variations in hypoxic dynamics observed in this study warrants further imaging work to examine cerebral capillary transit time heterogeneity (31) in patients with SCD and other chronic anemias.

REFERENCES:

1. Coyer SM. Anemia: Diagnosis and Management. *J Pediatr Heal Care*. 2005;19(6):380-385.
2. Kaiafa G, Savopoulos C, Kanellos I, et al. Anemia and stroke: Where do we stand? *Acta Neurol Scand*. 2017;135(6):596-602.
3. Kassim AA, Pruthi S, Day M, et al. Silent cerebral infarcts and cerebral aneurysms are prevalent in adults with sickle cell anemia. *Blood*. 2016;127(16):2038-2040.
4. Spivey JF, Uong EC, Strunk R, Boslaugh SE, DeBaun MR. Low daytime pulse oximetry reading is associated with nocturnal desaturation and obstructive sleep apnea in children with sickle cell anemia. *Pediatr Blood Cancer*. 2008;50(2):359-362.
5. Quinn CT, Sargent JW. Daytime steady-state haemoglobin desaturation is a risk factor for overt stroke in children with sickle cell anaemia. *Br J Haematol*. 2008;140(3):336-339.
6. Jöbsis FF. Noninvasive, infrared monitoring of cerebral and myocardial oxygen sufficiency and circulatory parameters. *Science*. 1977;198(4323):1264-1267.
7. Glover GH. Overview of Functional Magnetic Resonance Imaging. *Neurosurg Clin N Am*. 2011;22(2):133.
8. DeBaun MR, Gordon M, McKinstry RC, et al. Controlled Trial of Transfusions for Silent Cerebral Infarcts in Sickle Cell Anemia. *N Engl J Med*. 2014;371(8):699-710.
9. Coloigner J, Kim Y, Bush A, et al. Contrasting resting-state fMRI abnormalities from sickle and non-sickle anemia. Kassner A, ed. *PLoS One*. 2017;12(10):e0184860.
10. Holmes CJ, Hoge R, Collins L, Woods R, Toga AW, Evans AC. Enhancement of MR images using registration for signal averaging. *J Comput Assist Tomogr*. 1998;22(2):324-333.

11. Tatu L, Moulin T, Vuillier F, Bogousslavsky J. Arterial Territories of the Human Brain. *Front of Neurol Neurosci*. 2012;30:99-110.

12. Enzmann DR, Ross MR, Marks MP, Pelc NJ. Blood flow in major cerebral arteries measured by phase-contrast cine MR. *AJNR Am J Neuroradiol*. 1994;15(1):123-129.

13. Chai Y, Bush AM, Coloigner J, et al. White Matter Has Impaired Resting Oxygen Delivery in Sickle Cell Patients. *Am J Hematol*. 2019;94(4):467-474.

14. DeBaun MR, Kirkham FJ. Central nervous system complications and management in sickle cell disease. *Blood*. 2016;127(7):829-838.

15. Ohene-Frempong K, Weiner SJ, Sleeper LA, et al. Cerebrovascular Accidents in Sickle Cell Disease: Rates and Risk Factors and the Cooperative Study of Sickle Cell Disease. *Blood*. 1998;91(1):288-294.

16. Kinney TR, Sleeper LA, Wang WC, et al. Silent cerebral infarcts in sickle cell anemia: a risk factor analysis. The Cooperative Study of Sickle Cell Disease. *Pediatrics*. 1999;103(3):640-645.

17. Choi S, O'Neil SH, Joshi AA, et al. Anemia predicts lower white matter volume and cognitive performance in sickle and non-sickle cell anemia syndrome. *Am J Hematol*. 2019;94(10):1055-1065.

18. Inwald DP, Kirkham FJ, Peters MJ, et al. Platelet and leucocyte activation in childhood sickle cell disease: association with nocturnal hypoxaemia. *Br J Haematol*. 2000;111(2):474-481.

19. Sangkatumvong S, Khoo MCK, Kato R, et al. Peripheral Vasoconstriction and Abnormal Parasympathetic Response to Sighs and Transient Hypoxia in Sickle Cell Disease. *Am J Respir Crit Care Med*. 2011;184(4):474-481.

20. MacDonald ME, Berman AJL, Mazerolle EL, Williams RJ, Pike GB. Modeling hyperoxia-induced BOLD signal dynamics to estimate cerebral blood flow, volume and mean transit time. *Neuroimage*. 2018;178:461-474.

21. Huppert TJ, Hoge RD, Diamond SG, Franceschini MA, Boas DA. A temporal comparison of BOLD, ASL, and NIRS hemodynamic responses to motor stimuli in adult humans. *Neuroimage*. 2006;29(2):368-382.

22. Harris AD, Murphy K, Diaz CM, et al. Cerebral blood flow response to acute hypoxic hypoxia. *NMR Biomed*. 2013;26(12):1844-1852.

23. Poulin MJ, Liang PJ, Robbins PA. Dynamics of the cerebral blood flow response to step changes in end-tidal PCO2 and PO2 in humans. *J Appl Physiol*. 1996;81(3):1084-1095.

24. El Hasnaoui-Saadani R, Pichon A, Marchant D, et al. Cerebral adaptations to chronic anemia in a model of erythropoietin-deficient mice exposed to hypoxia. *Am J Physiol Integr Comp Physiol*. 2009;296(3):R801-R811.

25. Borgström L, Jóhannsson H, Siesjö BK. The Relationship between Arterial P_{O2} and Cerebral Blood Flow in Hypoxic Hypoxia. *Acta Physiol Scand*. 1975;93(3):423-432.

26. Kosinski PD, Croal PL, Leung J, et al. The severity of anaemia depletes cerebrovascular dilatory reserve in children with sickle cell disease: a quantitative magnetic resonance imaging study. *Br J Haematol*. 2017;176(2):280-287.

27. Santiago T V, Edelman NH, Fishman AP. The effect of anemia on the ventilatory response to transient and steady-state hypoxia. *J Clin Invest*. 1975;55(2):410-418.

28. Miao X, Choi S, Tamrazi B, et al. Increased brain iron deposition in patients with sickle cell disease: an MRI quantitative susceptibility mapping study. *Blood*. 2018;132(15):1618-1621.

29. Detterich JA, Kato RM, Rabai M, Meiselman HJ, Coates TD, Wood JC. Chronic transfusion therapy improves but does not normalize systemic and pulmonary vasculopathy in sickle cell disease. *Blood*. 2015;126(6):703-710.

30. Reckelhoff JF. Gender differences in the regulation of blood pressure. *Hypertension*. 2001;37(5):1199-1208.

31. Jespersen SN, Østergaard L. The Roles of Cerebral Blood Flow, Capillary Transit Time Heterogeneity, and Oxygen Tension in Brain Oxygenation and Metabolism. *J Cereb Blood Flow Metab*. 2012;32(2):264-277.

32. Østergaard L, Engedal TS, Aamand R, et al. Capillary transit time heterogeneity and flow-metabolism coupling after traumatic brain injury. *J Cereb Blood Flow Metab*. 2014;34(10):1585-1598.

33. Numaguchi Y, Haller JS, Humbert JR, et al. Cerebral blood flow mapping using stable Xenon-enhanced CT in sickle cell cerebrovascular disease. *Neuroradiology*. 1990;32(4):289-295.

34. Fields ME, Guilliams KP, Ragan DK, et al. Regional oxygen extraction predicts border zone vulnerability to stroke in sickle cell disease. *Neurology*. 2018;90(13):e1134-e1142.

35. Mandell DM, Han JS, Poublanc J, et al. Selective Reduction of Blood Flow to White Matter During Hypercapnia Corresponds With Leukoaraiosis. *Stroke*. 2008;39(7):1993-1998.

36. Sam K, Conklin J, Holmes KR, et al. Impaired dynamic cerebrovascular response to hypercapnia predicts development of white matter hyperintensities. 2016;11:896-801.

37. Binks AP, Cunningham VJ, Adams L, Banzett RB. Gray matter blood flow change is unevenly distributed during moderate isocapnic hypoxia in humans. *J Appl Physiol*.

2008;104(1):212-217.

38. Poublanc J, Han JS, Mandell DM, et al. Vascular Steal Explains Early Paradoxical Blood Oxygen Level-Dependent Cerebrovascular Response in Brain Regions with Delayed Arterial Transit Times. *Cerebrovasc Dis Extra*. 2013;3(1):55-64.

39. Von Sarnowski B, Schminke U, Grittner U, et al. Posterior versus Anterior Circulation Stroke in Young Adults: A Comparative Study of Stroke Aetiologies and Risk Factors in Stroke among Young Fabry Patients (sifap1). *Cerebrovasc Dis*. 2017;43(3-4):152-160.

40. Xu F, Li W, Liu P, et al. Accounting for the role of hematocrit in between-subject variations of MRI-derived baseline cerebral hemodynamic parameters and functional BOLD responses. *Hum Brain Mapp*. 2018;39(1):344-353.

Tables:

Table 1. Patient demographic and hematologic data. Bold letterings indicate statistical significance ($p<0.05$).

	CTL (N=31)	**SCD** (N=26)	**ACTL** (N=15)	***p*-value** (SCD vs. CTL)	***p*-value** (ACTL vs. CTL)	***p*-value** (SCD vs. ACTL)
Age (Years)	28±12.3	21±8.2	22±5.8	**0.02**	0.13	0.65
Sex	7M, 24F	14M, 12F	5M, 10F	**0.03**	0.70	0.18
Hemoglobin Electrophoresis	15AA, 16AS	19SS, 5SC, 2Sβ_0	13AA, 2AE			
Cerebral Blood Flow (mL/100g/min)	62±10.9	95±22.6	85±12.7	**<0.01**	**<0.01**	0.07
Transfusion	0/31	12/26	12/15	**<0.01**	**<0.01**	**<0.01**
SCI presence	3/31	9/26	2/15	**0.03**	0.94	0.09
Hemoglobin (g/dL)	13±1.4	10±1.9	10±1.5	**<0.01**	**<0.01**	0.78
Hematocrit (%)	39±3.6	29±4.3	31±3.9	**<0.01**	**<0.01**	0.10
White Blood Cell ($x10^3$)	6±2.0	10±4.7	6±1.9	**<0.01**	0.91	**<0.01**
Platelet Count ($x10^3/\mu L$)	245±53.8	292±112.6	255±111.8	0.10	0.93	0.21
Reticulocytes (%)	1±0.6	9±5.3	2±2.8	0.11	0.99	**0.03**
S-cells Fraction (%)	0	44±30.1	0	**<0.01**	1.00	**<0.01**
Fetal Hemoglobin (%)	1±2.1	6±7.8	2±2.3	**<0.01**	0.66	**0.02**
Cell-free Hemoglobin (%)	6±5.0	18±18.1	20±24.0	**<0.01**	**<0.01**	0.62

Table 2. Group average NIRS and BOLD desaturation parameters. Bold letterings indicate statistical significance (p<0.05).

	CTL (N=31)	**SCD** (N=26)	**ACTL** (N=15)	***p*-value** (SCD vs. CTL)	***p*-value** (ACTL vs. CTL)	***p*-value** (SCD vs. ACTL)
$\Delta_{DeoxyHb}$ (μmol)	1±0.4	2±0.6	1±0.6	**0.03**	0.21	0.69
Δ_{OxyHb} (μmol)	1±0.6	2±0.5	2±0.9	0.22	0.08	0.37
$T½_{DeoxyHb}$ (s)	24±8.0	18±8.5	17±5.5	0.06	**0.03**	0.59
$T½_{OxyHb}$ (s)	19±10.2	12±5.9	16±8.9	**0.03**	0.53	0.32
$TTP_{DeoxyHb}$ (s)	25±4.1	21±5.3	21±6.3	0.07	0.13	0.89
TTP_{OxyHb} (s)	26±9.5	20±3.7	25±6.7	**0.02**	0.89	0.09
$R_{TotalHb}$ (μmol)	0.08±0.074	0.05±0.061	0.03±0.059	0.28	0.09	0.38
Δ_{BOLD} (%)	6±2.1	8±2.6	8±2.6	**<0.01**	**0.03**	0.94
$T½_{BOLD}$ (s)	16±3.5	13±3.0	15±3.6	**<0.01**	0.35	**0.03**
TTP_{BOLD} (s)	23±3.7	21±4.5	23±3.7	0.27	0.96	0.37

Table 3. Predictors of $T½_{BOLD}$, TTP_{BOLD} and Δ_{BOLD}. Bold letterings indicate retention on multivariate analysis. β is the standardized regression coefficient for predictors retained on the multivariate model, and r^2 is the coefficient of determination for the univariate regression.

Predictor	$T½_{BOLD}$	TTP_{BOLD}	Δ_{BOLD}
Cerebral Blood Flow (mL/100g/min)	**r^2=0.22, p<0.01, β = –0.47**	–	r^2=0.16, p<0.01
Age (years)	r^2=0.09, p=0.02	–	**r^2=0.14, p<0.01 β = –0.37**
Sex (male = 1)	–	**r^2=0.08, p=0.03, β = –0.28**	–
Hemoglobin (g/dL)	r^2=0.17, p<0.01	–	r^2=0.09, p=0.02
Transfusion Status	r^2=0.09, p=0.02	–	r^2=0.08, p=0.03
White Blood Cells (x10^3)	**r^2=0.21, p<0.01, β = –0.46**	–	**r^2=0.15, p<0.01, β = 0.39**
Reticulocytes (%)	r^2=0.05, p=0.08	–	–
S-cells fraction (%)	r^2=0.09, p=0.02	–	–
Fetal Hemoglobin (%)	r^2=0.07, p=0.04	–	–
Cell-free Hemoglobin (mg/dL)	r^2=0.09, p=0.02	**r^2=0.07, p=0.03, β = –0.27**	–

Table 4. Two-tailed Student's paired *t*-tests were used to compare desaturation depth and timing within infarct-prone white matter and normal appearing white matter. Bold letterings indicate statistical significance ($p<0.05$).

Hb-corrected *t*-maps		**Infarct-prone WM**	**Normal Appearing WM**	*p*-value
$T½_{BOLD}$	SCI–	–0.3 ± 0.47	–0.4 ± 0.55	0.14
	SCI+	–0.4 ± 0.81	–0.5 ± 1.02	**<0.01**
TTP_{BOLD}	SCI–	0.4 ± 0.42	0.4 ± 0.46	**0.03**
	SCI+	–0.6 ± 0.67	–0.4 ± 0.75	**<0.01**
Δ_{BOLD}	SCI–	0.6 ± 0.49	0.6 ± 0.49	**<0.01**
	SCI+	1.2 ± 0.86	1.4 ± 0.88	**<0.01**

Figure Legends:

Figure 1. Experimental setup for transient hypoxia gas paradigm and concurrent S_pO_2, NIRS and BOLD MRI acquisitions.

Figure 2. Transient hypoxia model and curve fitting for S_pO_2, BOLD and NIRS signals. (**A**) Representative recording of S_pO_2 signal during the hypoxia challenge. (**B**) S_pO_2 signal recording from the same patient *prior* to gas challenge while patient was sleeping during anatomic scanning. (**C**) Representative recordings of S_pO_2, global BOLD, NIRS OxyHb and DeoxyHb changes during the hypoxia challenge. (**D**) Example of curve fitting for a typical DeoxyHb signal.

Figure 3. Correlations between BOLD and NIRS hypoxic depths and hemoglobin levels. Correlations between hemoglobin levels with (**A**) baseline recovery $R_{TotalHb}$ and (**B**) Δ_{BOLD} demonstrated the role of anemia in compromised hypoxic and vasodilatory response in chronic anemia. Strong inter-modality correlations between BOLD desaturation depth Δ_{BOLD} and NIRS (**C**) $\Delta_{DeoxyHb}$ and (**D**) Δ_{OxyHb} further affirmed the use of these signals as estimates for global cerebral tissue oxygenation.

Figure 4. Mean, effect size, and hemoglobin correlation Δ_{BOLD} maps in three patient groups. (**A**) Average desaturation depth Δ_{BOLD} showed globally higher desaturation depth in anemic patients compared to healthy controls, more so in grey matter than white matter. Representative silent cerebral infarcts are illustrated as white labels on these maps. (**B**) Cohen's *d*-maps of Δ_{BOLD} demonstrated larger hypoxic effect size in anemic patients compared to controls.

Figure 5. Two-sample *t*-maps of Δ_{BOLD}, $T1/2_{BOLD}$ and TTP_{BOLD} between SCD patients and healthy controls. (**A**) Two-sample *t*-maps of desaturation depth Δ_{BOLD}, time constants $T1/2_{BOLD}$ and TTP_{BOLD} between SCD patients and healthy controls with correction for age and sex showed areas of high variability in hypoxic response co-localized with regions of high silent-stroke risk. (**B**) Parameter *t*-maps corrected for hemoglobin levels in addition to age and sex showed that anemia accounted for a large degree of group discrepancy. The disparity between parameter *t*-maps corrected for hemoglobin level and subdivided into (**C**) SCI– subgroup and (**D**) SCI+ subgroup compared to healthy controls demonstrated that patients with silent infarcts have a higher degree of spatial heterogeneity in their regional BOLD hypoxic responses. Representative silent cerebral infarcts are illustrated as white labels on these maps.

Figure 6. Two-sample *t*-maps of Δ_{BOLD}, $T1/2_{BOLD}$ and TTP_{BOLD} between ACTL subjects and healthy controls. Age-sex-corrected (**A**) and age-sex-hemoglobin-corrected (**B**) two-sample *t*-maps of Δ_{BOLD}, $T1/2_{BOLD}$ and TTP_{BOLD} between non-sickle anemia patients and healthy controls showed that correcting for hemoglobin in this patient population produced a modest effect on reducing the variations between anemic patients and controls. Representative silent cerebral infarcts are illustrated as white labels on these maps.

Figures:

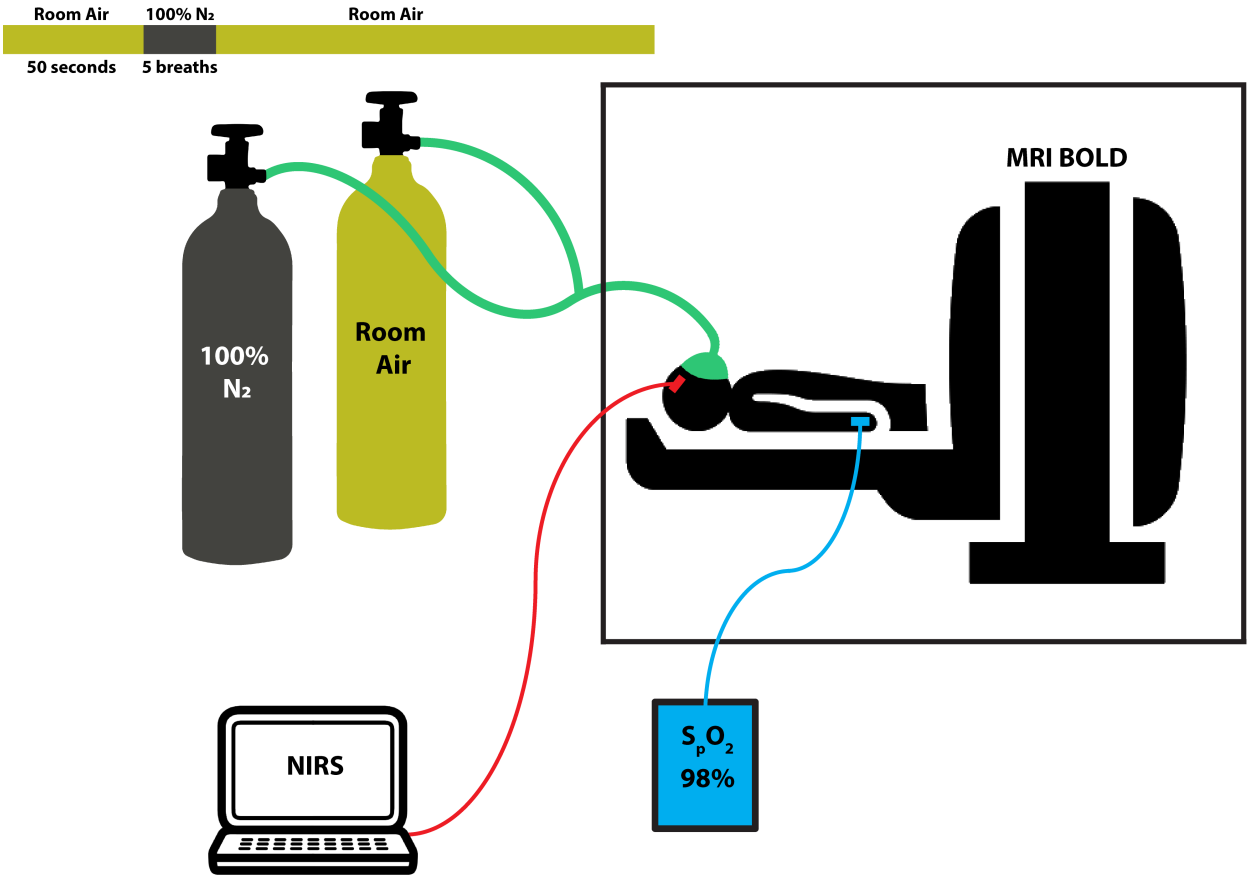


Figure 1. Experimental setup for transient hypoxia gas paradigm and concurrent S_pO_2, NIRS and BOLD MRI acquisitions.

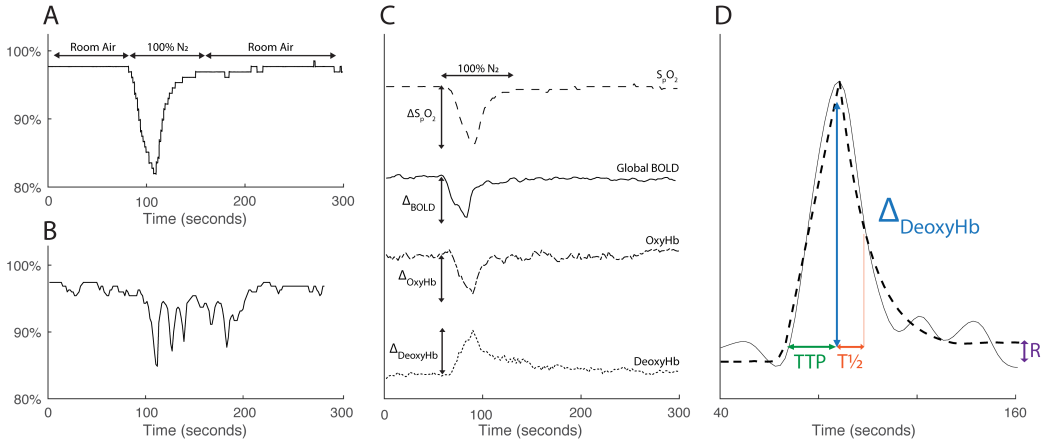


Figure 2. Transient hypoxia model and curve fitting for S_pO_2, BOLD and NIRS signals. (A) Representative recording of S_pO_2 signal during the hypoxia challenge. (B) S_pO_2 signal recording from the same patient *prior* to gas challenge while patient was sleeping during anatomic scanning. (C) Representative recordings of S_pO_2, global BOLD, NIRS OxyHb and DeoxyHb changes during the hypoxia challenge. (D) Example of curve fitting for a typical DeoxyHb signal.

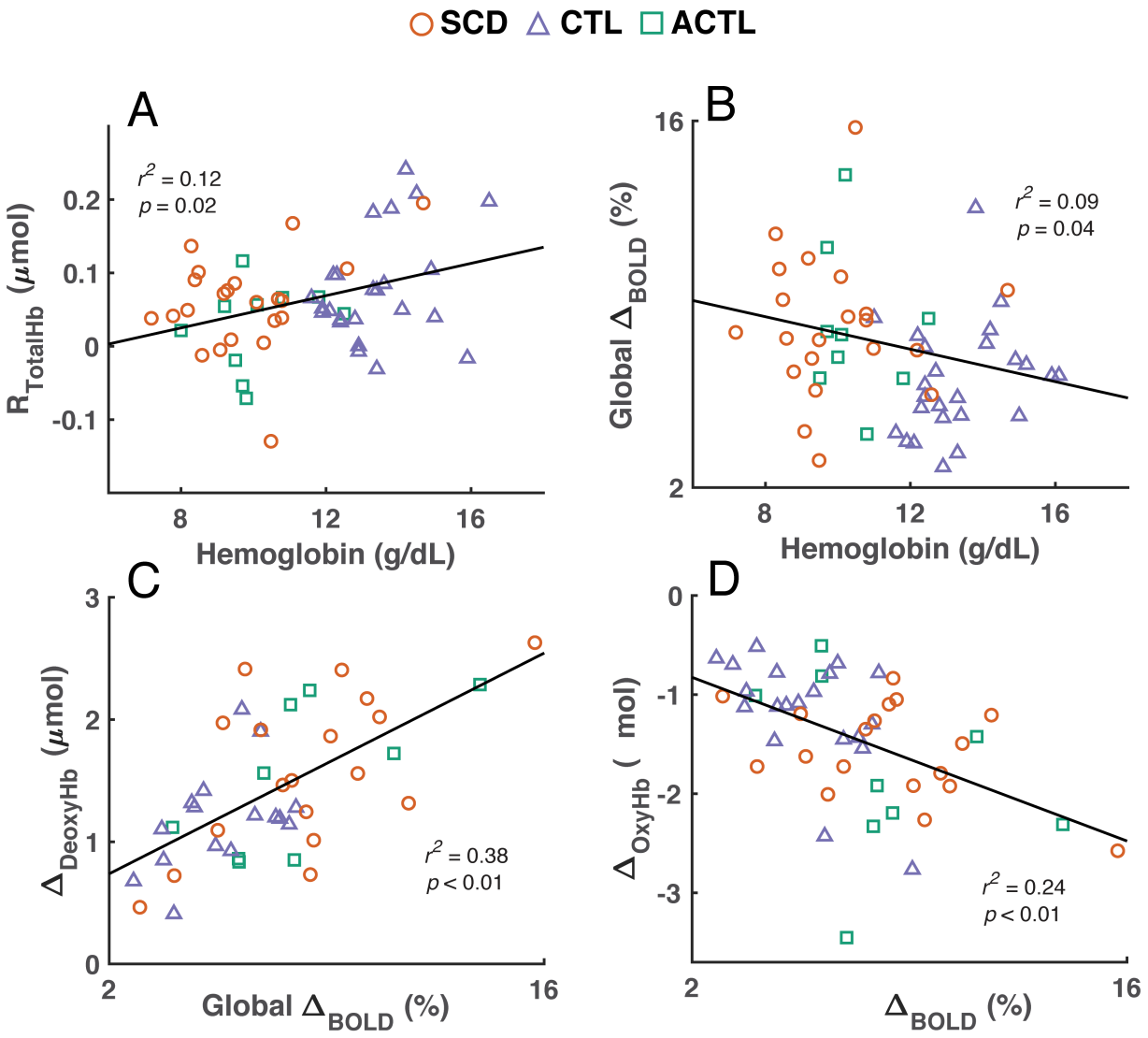


Figure 3. Correlations between BOLD and NIRS hypoxic depths and hemoglobin levels. Correlations between hemoglobin levels with (A) baseline recovery $R_{TotalHb}$ and (B) Δ_{BOLD} demonstrated the role of anemia in compromised hypoxic and vasodilatory response in chronic anemia. Strong inter-modality correlations between BOLD desaturation depth Δ_{BOLD} and NIRS (C) $\Delta_{DeoxyHb}$ and (D) Δ_{OxyHb} further affirmed the use of these signals as estimates for global cerebral tissue oxygenation.

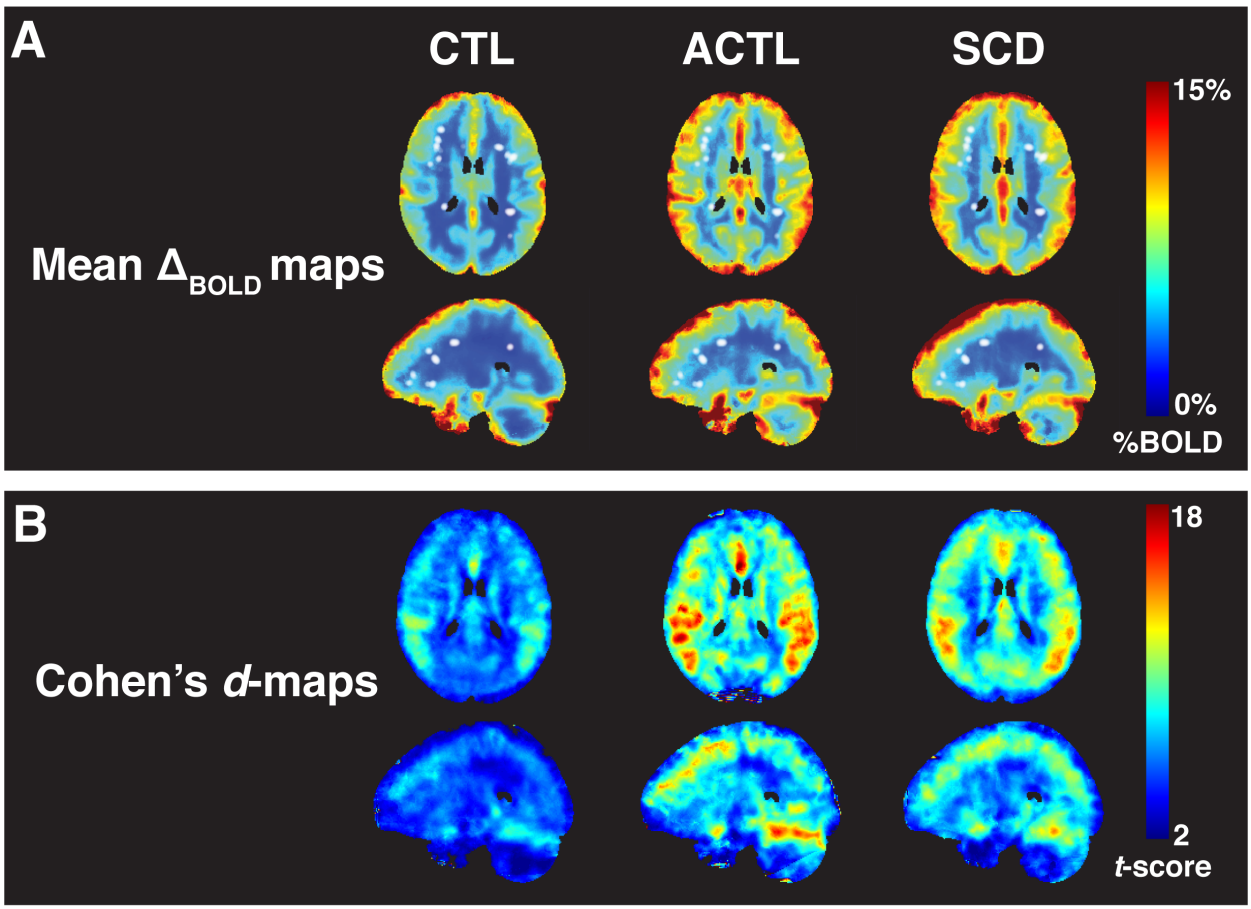


Figure 4. Mean, effect size, and hemoglobin correlation Δ_{BOLD} maps in three patient groups. (A) Average desaturation depth Δ_{BOLD} showed globally higher desaturation depth in anemic patients compared to healthy controls, more so in grey matter than white matter. Representative silent cerebral infarcts are illustrated as white labels on these maps. (B) Cohen's *d*-maps of Δ_{BOLD} demonstrated larger hypoxic effect size in anemic patients compared to controls.

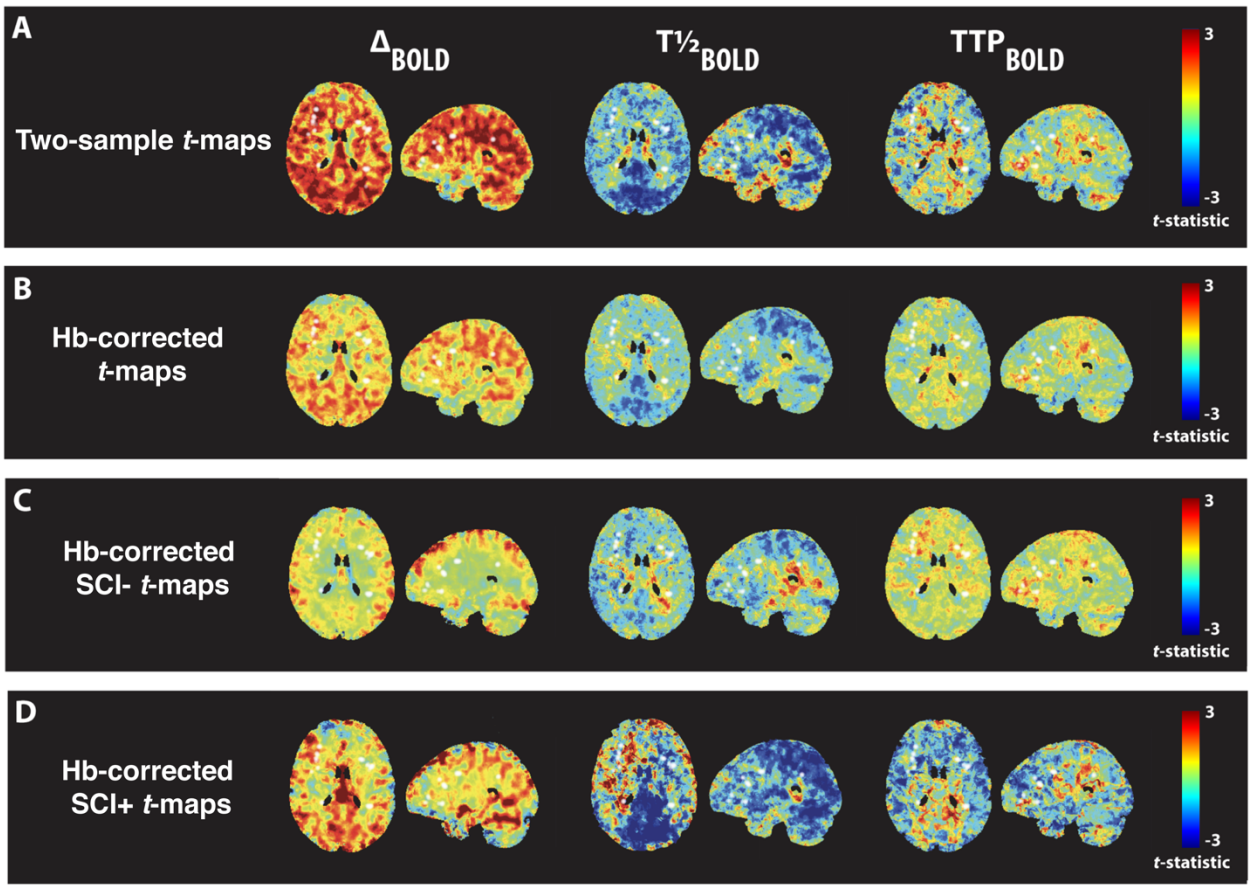


Figure 5. Two-sample *t*-maps of Δ_{BOLD}, $T½_{BOLD}$ and TTP_{BOLD} between SCD patients and healthy controls. (A) Two-sample *t*-maps of desaturation depth Δ_{BOLD}, time constants $T½_{BOLD}$ and TTP_{BOLD} between SCD patients and healthy controls with correction for age and sex showed areas of high variability in hypoxic response co-localized with regions of high silent-stroke risk. (B) Parameter *t*-maps corrected for hemoglobin levels in addition to age and sex showed that anemia accounted for a large degree of group discrepancy. The disparity between parameter *t*-maps corrected for hemoglobin level and subdivided into (C) SCI– subgroup and (D) SCI+ subgroup compared to healthy controls demonstrated that patients with silent infarcts have a higher degree of spatial heterogeneity in their regional BOLD hypoxic responses. Representative silent cerebral infarcts are illustrated as white labels on these maps.

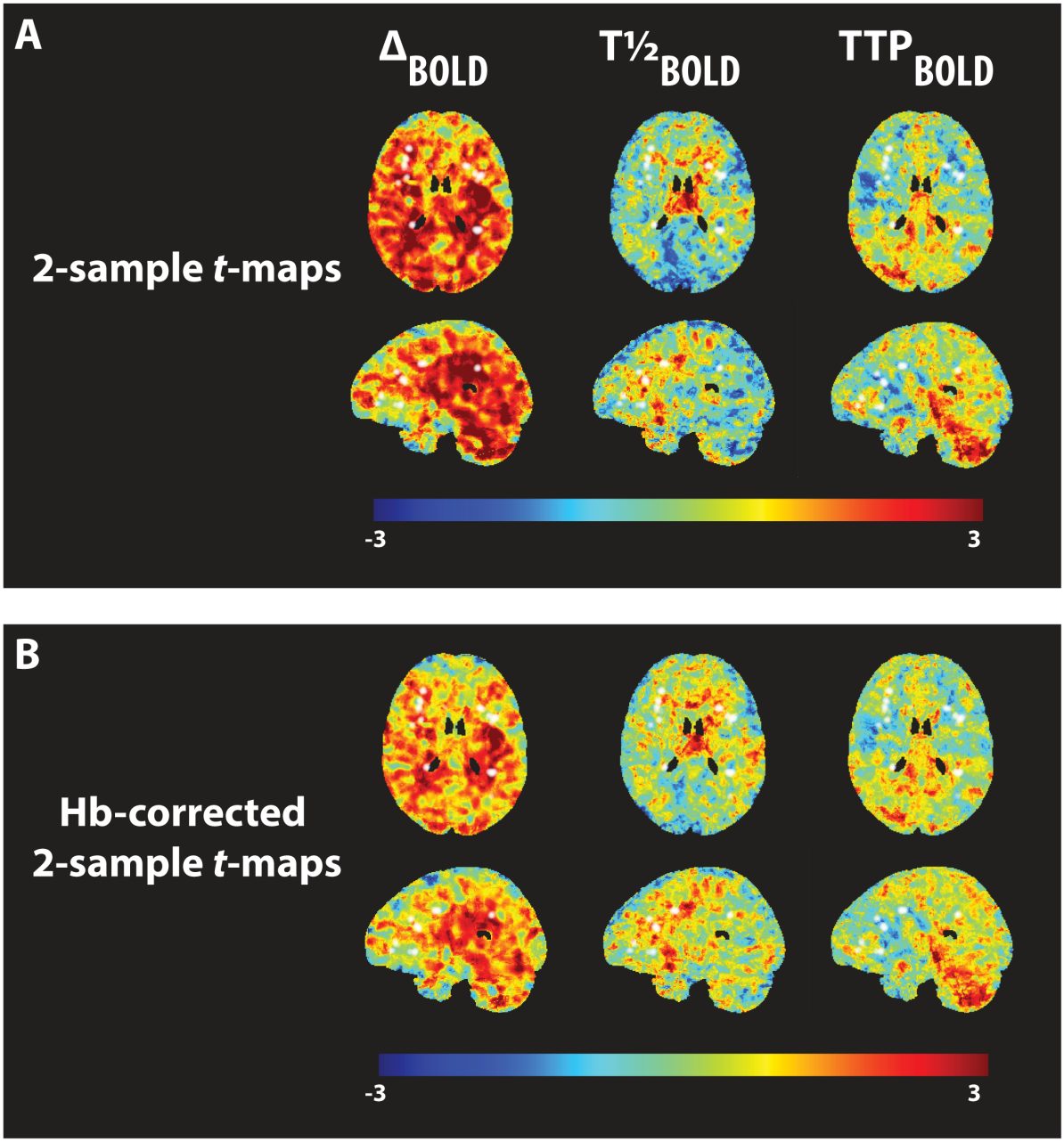


Figure 6. Two-sample *t*-maps of Δ_{BOLD}, $T½_{BOLD}$ and TTP_{BOLD} between ACTL subjects and healthy controls. Age-sex-corrected (A) and age-sex-hemoglobin-corrected (B) two-sample *t*-maps of Δ_{BOLD}, $T½_{BOLD}$ and TTP_{BOLD} between non-sickle anemia patients and healthy controls showed that correcting for hemoglobin in this patient population produced a modest effect on reducing the variations between anemic patients and controls. Representative silent cerebral infarcts are illustrated as white labels on these maps.